

# Single-Carrier Waveform Design for Joint Sensing and Communication

Ayoub Ammar Boudjelal, Rania Yasmine Bir, and Hüseyin Arslan, *Fellow, IEEE*

**Abstract**—The emergence of 6G wireless networks demands solutions that seamlessly integrate communication and sensing. This letter proposes a novel waveform design for joint sensing and communication (JSAC) systems, combining single-carrier interleaved frequency division multiplexing (SC-IFDM), a 5G communication candidate signal, with frequency modulated continuous wave (FMCW), widely used for sensing. The proposed waveform leverages the sparse nature of FMCW within SC-IFDM to achieve orthogonal integration in three steps: SC-IFDM symbols are allocated alongside the sparse FMCW, followed by the SC-IFDM transform into the time domain, and a cyclic prefix (CP) is applied in which phase shifts are introduced to the FMCW. Additionally, an enhanced channel estimation method is incorporated to boost system performance. Simulation results demonstrate the proposed waveform’s ability to deliver high-resolution sensing and superior communication performance, surpassing traditional multicarrier designs.

**Index Terms**—JSAC, OFDM, FMCW, SC-IFDM, waveform.

## I. INTRODUCTION

THE joint sensing and communication (JSAC) paradigm is increasingly recognized as essential for deploying efficient sixth Generation (6G) networks. By integrating communication and sensing functionalities, JSAC enables network nodes to not only transmit data but also perceive their environment, leading to improved system reliability, decision-making, and overall resource efficiency [1], [2]. However, as device density increases, interference becomes a pressing issue, highlighting the need for novel sensing and communication waveform designs to manage resources effectively while ensuring interference mitigation and supporting the stringent requirements of real-time sensing and communication in 6G [1].

Several signal designs have been presented to perform both sensing and communication, such as orthogonal frequency division multiplexing (OFDM) and orthogonal time-frequency space (OTFS) [3]. These multicarrier signals demonstrate estimation accuracy comparable to that of frequency modulated continuous wave (FMCW), a widely used automotive radar waveform [4], [5], while simultaneously achieving high communication rates. These findings indicate that joint radar estimation and communication can be efficiently performed without compromising throughput or accuracy.

In [6] [7], OTFS and FMCW signals are combined to achieve high data rates and low-complexity sensing. However,

OTFS suffers from high peak to average power ratio (PAPR), reducing power efficiency and requiring pre-coding techniques [8]. While the coexistence aims to simplify sensing and increase throughput, it introduces complexity by relying on radar processing for delay and Doppler shifts, undermining OTFS’s benefits. In [9], the coexistence of OFDM and FMCW achieves comparable sensing performance, but reallocating diagonal elements disrupts orthogonality, degrading communication performance. Additionally, the communication performance was only tested in static channels, making it impractical for mobile environments.

In single-carrier systems, single-carrier interleaved frequency division multiplexing (SC-IFDM), interpreted as a linearly precoded OFDM in which the occupied sub-carriers are equally spaced over the entire bandwidth [10], offers a key advantage over multicarrier signals where lower PAPR level can be achieved. This low PAPR level simplifies the transmitter design for user devices and makes it ideal for uplink transmission in LTE systems [11], [12] and 6G applications.

Building on the strengths of SC-IFDM, this letter introduces a novel waveform design for JSAC systems by integrating FMCW signal orthogonally with SC-IFDM signaling. The key contributions of this work are:<sup>1</sup>

- A novel SC-IFDM-FMCW signal is proposed, enabling simultaneous communication and sensing. This design leverages the sparsity of FMCW in the discrete Fourier transform (DFT) domain to diagonally integrate it with the SC-IFDM signal, minimizing interference and simplifying the receiver architecture for both functions.
- A novel channel estimation method is proposed, using the integrated FMCW signal as a pilot in the DFT domain. This eliminates the need for guard bands between pilot and data symbols, leveraging the chirp’s sparsity in the DFT domain rather than the frequency domain, thereby boosting spectral efficiency.
- Simulation results demonstrate that the proposed waveform achieves high-resolution sensing and outperforms JSAC waveforms like OFDM-FMCW and OTFS-FMCW in communication performance.

The authors are with the Department of Electrical and Electronics Engineering, Istanbul Medipol University, Istanbul, 34810, Turkey (e-mail: ayoub.ammar@std.medipol.edu.tr; rania.bir@std.medipol.edu.tr; huseyinarslan@medipol.edu.tr).

<sup>1</sup>*Notation:* Bold uppercase  $\mathbf{A}$ , bold lowercase  $\mathbf{a}$ , and unbold letters  $A, a$  denote matrices, column vectors, and scalar values, respectively.  $(\cdot)^{-1}$  denote the inverse operators.  $\delta(\cdot)$  denotes the Dirac-delta function.  $\mathbb{C}^{M \times N}$  denotes the space of  $M \times N$  complex-valued matrices.

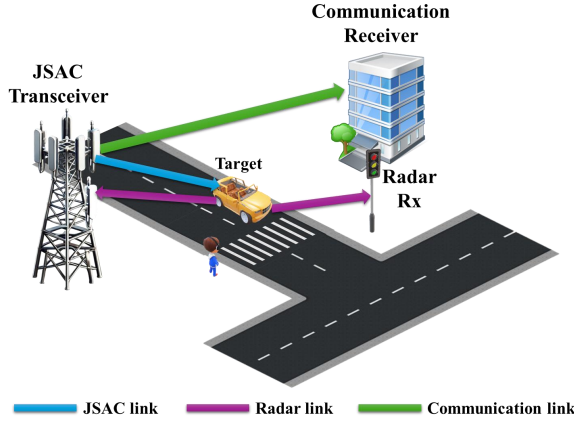


Fig. 1. Illustration of the JSAC network.

## II. THE PROPOSED WAVEFORM DESIGN

In this section, we model the SC-IFDM and FMCW signaling and describe how the sparse representation of FMCW integrates with SC-IFDM to create the proposed SC-IFDM-FMCW waveform for JSAC systems. The proposed JSAC system performs dual functions, serving as a mono-static radar for sensing and a communication transmitter. Additionally, other separate systems in the environment may act as bi-static radars for sensing, as illustrated in Fig. 1. By transmitting the proposed SC-IFDM-FMCW waveform, the system simultaneously detects radar echoes for sensing while transmitting data to a dedicated receiver, ensuring there is no interference between the sensing and communication functionalities.

### A. SC-IFDM Signal Model

Assuming  $M \times N$  data symbols are modulated using SC-IFDM by mapping them to  $N$  DFT blocks, each of size  $M$ , and interleaving the output of these DFT blocks before applying the final  $MN$ -point inverse discrete Fourier transform (IDFT), the resulting signal  $s^{\text{SC-IFDM}}(p)$ , with  $\{X^{\text{SC-IFDM}}(k, l)\}$  for  $k = 0, \dots, N-1$  and  $l = 0, \dots, M-1$ , is expressed as [13]

$$s^{\text{SC-IFDM}}(p) = \frac{1}{\sqrt{N}} \sum_{k=0}^{N-1} X^{\text{SC-IFDM}}(k, [p]_M) e^{j2\pi \frac{k}{MN} p}, \quad (1)$$

for  $p = 0, 1, \dots, MN-1$ . We can reformulate (1) by setting  $p = l + nM$ , such that  $n = 0, \dots, N-1$ . Substituting this into the expression, we get

$$s^{\text{SC-IFDM}}(l + nM) = \frac{1}{\sqrt{N}} \sum_{k=0}^{N-1} X^{\text{SC-IFDM}}(k, l) e^{j2\pi \frac{k(l+nM)}{MN}}. \quad (2)$$

### B. FMCW Signal Model

Consider a linear FMCW signal,  $s^{\text{FMCW}}(t)$ , which sweeps linearly across bandwidth  $B_c$  over a time duration  $T_c$ . The time-domain representation of  $s^{\text{FMCW}}(t)$  is expressed as [14]

$$s^{\text{FMCW}}(t) = e^{j\pi\eta t^2}, \quad 0 \leq t < T_c, \quad (3)$$

where  $\eta = B_c/T_c$  is the FMCW rate. Here,  $\eta$ ,  $T_c$ , and  $B_c \in \mathbb{R}$ . Assume that the time-bandwidth product  $MN = \eta T_c^2$  is a

nonzero integer. The critically sampled FMCW pulse is then formed by sampling at discrete points  $t = \frac{p}{MN} T_c$ , resulting in

$$s^{\text{FMCW}}(p) = e^{j\pi \frac{p^2}{MN}}, \quad 0 \leq p < MN. \quad (4)$$

### C. SC-IFDM to FMCW

Taking  $p = l + nM$ , the discrete FMCW signal in (4) can be represented using SC-IFDM structure after applying the inverse transform of (2). This yields the following expression

$$\begin{aligned} X_{\text{SC-IFDM}}^{\text{FMCW}}(k, l) &= \frac{1}{\sqrt{N}} \sum_{n=0}^{N-1} s^{\text{FMCW}}(l + nM) e^{-j2\pi \frac{k(l+nM)}{MN}} \\ &= \frac{e^{j\pi(\frac{l^2}{MN})} \omega_k^l}{\sqrt{N}} \sum_{n=0}^{N-1} e^{j2\pi \frac{(\frac{M}{2}n^2 + (l-k)n)}{N}}, \end{aligned} \quad (5)$$

where  $\omega_k^l = e^{j2\pi(\frac{-kl}{MN})}$ . Note that  $e^{j\pi n} = 1$  for even  $n$  and  $-1$  for odd  $n$ . Similarly,  $n^2$  is even when  $n$  is even and odd when  $n$  is odd. Given that  $M \in \mathbb{Z}$ , we find that  $e^{j\pi(Mn^2)} = (-1)^{Mn^2} = (-1)^{Mn}$ . Incorporating this into (5), we get

$$X_{\text{SC-IFDM}}^{\text{FMCW}}(k, l) = \frac{e^{j\pi(\frac{l^2}{MN})} \omega_k^l}{\sqrt{N}} \sum_{n=0}^{N-1} e^{j2\pi \frac{(\frac{M}{2}n^2 + (l-k)n)}{N}}. \quad (6)$$

The elements of the matrix  $X_{\text{SC-IFDM}}^{\text{FMCW}}(k, l)$  are nonzero only when  $[\frac{M}{2} + l - k]_N = 0$  leading to a sparsity condition where the matrix is nonzero for certain values of  $l$ . Specifically,  $X_{\text{SC-IFDM}}^{\text{FMCW}}(k, l)$  reduced to  $s^{\text{FMCW}}(l) \omega_k^l$  for the valid solutions corresponding to each  $l = 0, \dots, M-1$ . This results in a sparse matrix representation, where only  $M$  nonzero elements exist in the DFT-based space of the SC-IFDM. Thus, FMCW signaling can be efficiently generated using SC-IFDM by selecting the first  $M$  samples from  $s^{\text{FMCW}}$  according to this sparsity condition. This approach provides a computationally efficient way to combine the benefits of FMCW and SC-IFDM for JSAC systems. Similarly, a down FMCW chirp is represented using SC-IFDM structure as

$$X_{\text{SC-IFDM}}^{\text{FMCW}'}(k, l) = \frac{e^{-j\pi(\frac{l^2}{MN})} \omega_k^l}{\sqrt{N}} \sum_{n=0}^{N-1} e^{-j2\pi \frac{(\frac{M}{2}n^2 + (l+k)n)}{N}}. \quad (7)$$

### D. Proposed JSAC Signal

To generate the proposed JSAC signal  $X^{\text{comb}}(k, l)$ , which integrates SC-IFDM and FMCW signals in an orthogonal manner, a specific allocation is employed. First, the SC-IFDM signal is constructed by setting zeros at the indices where  $[\frac{M}{2} + l - k]_N$ , while the FMCW signal is mapped to these zero positions. This ensures orthogonality between the two signals. The combined signal is defined as

$$X^{\text{comb}}(k, l) = \begin{cases} \sqrt{\psi} s^{\text{FMCW}}(l) \omega_k^l, & [\frac{M}{2} + l - k]_N = 0 \\ X^{\text{SC-IFDM}}(k, l), & \text{otherwise,} \end{cases} \quad (8)$$

where  $\psi$  is a design parameter representing the power assigned to FMCW signal that will be used for sensing and also as pilots for channel estimation. Next, the combined signal  $X^{\text{comb}}(k, l)$  is transformed into the time-domain signal  $s^{\text{comb}}(l + nM)$  using the inverse transform from (2). Fig 2 illustrates the implementation, FMCW samples are allocated to the proper indices of each DFT block of the SC-IFDM. Finally, the

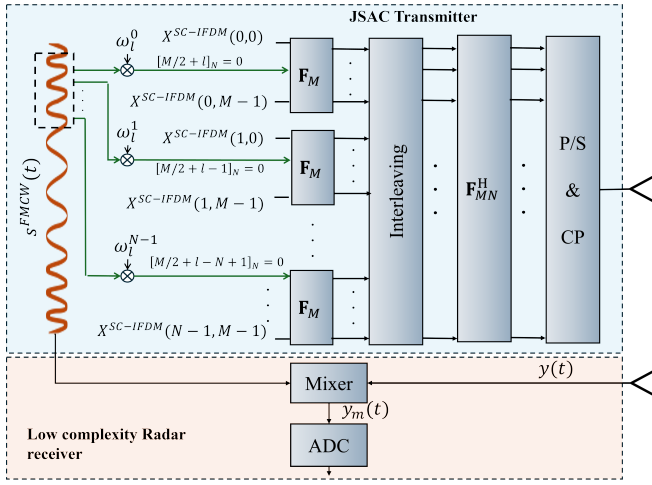


Fig. 2. The proposed SC-IFDM-FMCW transceiver design.

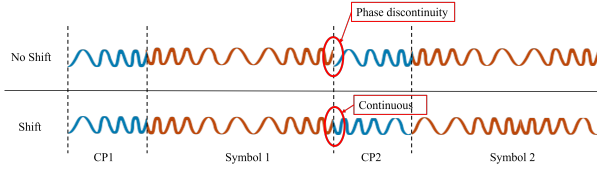


Fig. 3. CP addition before and after phase shift.

signal undergoes cyclic prefix (CP) insertion to ensure channel circularity. However, the potential discontinuity introduced by the CP leads to discontinuities between the  $i$ -th and the  $(i+1)$ -th FMCW signal, which decreases the sensing performance. Therefore, a proper time shift needs to be introduced to the  $i$ -th FMCW in the DFT domain to compensate for the CP duration  $L_{cp}$ . The  $i$ -th FMCW with the shift can be given as

$$X_{SC-IFDM}^{FMCW,i}(k, l) = \frac{s^{FMCW}(l - iL_{cp})\omega_k^l}{\sqrt{N}} \sum_{n=0}^{N-1} e^{j2\pi \left(\frac{M}{2} + l - k - iL_{cp}\right) \frac{n}{N}}. \quad (9)$$

Note that shifting the FMCW signal in time by the CP duration is a straightforward operation in SC-IFDM. This is achieved by taking the  $(l - iL_{cp})$  samples from the FMCW signal and placing them in the indices following  $[\frac{M}{2} + l - k - iL_{cp}]_N = 0$ . Fig.3 illustrates how this time shift ensures that the FMCW signal remains continuous after adding the CP. As a result, no additional processing or CP removal is required at the radar receiver side, allowing the signal to be directly mixed in the analog domain. This approach results in a low-complexity radar receiver design, as depicted in Fig. 2.

### III. CHANNEL

#### A. FMCW Processing

Consider a radar channel that models  $Q$  targets with range  $d_q$  and velocity  $v_q$  as follows

$$h(\tau, \nu) = \sum_{q=0}^{Q-1} h_q \delta(t - \tau_q) e^{j2\pi \nu_q (t - \tau_q)}, \quad (10)$$

where  $h_q$  is the complex channel gain corresponding to the  $q$ -th path,  $\tau_q = 2d_q/c$  denotes the round-trip delay,  $\nu_q = 2v_q f_c/c$  is the Doppler shift,  $f_c$  is the carrier frequency, and  $c$  is the speed of light. The radar channel's output is then expressed as

$$y(t) = \sum_{q=0}^{Q-1} h_q s^{comb}(t - \tau_q) e^{j2\pi \nu_q (t - \tau_q)}. \quad (11)$$

To extract the beat frequency  $f_B$  and the Doppler shift  $f_D$ , which carries the information about the time delay and Doppler shift induced by the targets, the received reflected signal is mixed with the conjugate of the transmitted chirp,  $\text{conj}(s^{FMCW})$ . For an up-chirp, the output is

$$y_m(t) = \sum_{q=0}^{Q-1} \tilde{h}_q e^{j2\pi(-\eta\tau_q + \nu_q)t} + I(t), \quad (12)$$

where  $\tilde{h}_q = h_q e^{j\pi\eta\tau_q^2} e^{-j2\pi\nu_q\tau_q}$  is the complex amplitude of the  $q$ -th path,  $\eta$  is the chirp slope, and  $I(t)$  is the interference from SC-IFDM which can be given as

$$I(t) = w(t) + \sum_{q=0}^{Q-1} h_q s^{SC-IFDM}(t - \tau_q) e^{j2\pi\nu_q(t - \tau_q)} \cdot e^{-j\pi\eta t^2}. \quad (13)$$

The radar data obtained from the up-chirp, as outlined in [15], is expressed as  $f_{bu} = f_B - f_D$ . Similarly, processing the down-chirp results in  $f_{bd} = f_B + f_D$ . These frequencies are used to calculate the range and velocity.

#### B. Communication channel

Consider a doubly selective  $R$ -tap channel, which can be expressed in discrete time domain as

$$h(p) = \sum_{r=0}^{R-1} h_r e^{j2\pi \frac{k_r(p-l_r)}{MN}} \delta(p - l_r), \quad (14)$$

where  $h_r$  denote the complex channel coefficient, while  $l_r$  and  $k_r$  represent the integer delay and Doppler shifts introduced by the channel, respectively. The received signal is given as

$$Y^{comb}(k, l) = \sum_{r=0}^{R-1} h_r e^{j2\pi \frac{k_r}{N} \frac{l-l_r}{M}} \Lambda_r(k, l) \times X^{comb}([k - k_r]_N, [l - l_r]_M) + W(k, l), \quad (15)$$

where  $\Lambda_r(k, l)$  is defined as 1 for  $l_r \leq l \leq M$  and as  $e^{-j2\pi \frac{k}{N}}$  for  $0 \leq l \leq l_r$ , and  $W(k, l)$  is additive white Gaussian noise of zero mean and variance  $\sigma^2$ . It is demonstrated that any delay or Doppler shift introduces a shift in both the data and chirp components. Since channel estimation relies on the chirp in the DFT domain, this causes interference between the data and chirp, ultimately degrading the accuracy of the channel estimation. The interfered chirp elements in the received signal,  $Y_{dp}$ , can be extracted by satisfying the condition  $[\frac{M}{2} + l + k_r - l_r - k]_N = 0$ , leading to the following result given as

$$Y_{dp}(k, l) = Y^{FMCW}(k, l) + \underbrace{Y^{SC-IFDM}(k, l)}_{\text{data to pilot interference}} + \underbrace{W(k, l)}_{\text{noise}}, \quad (16)$$

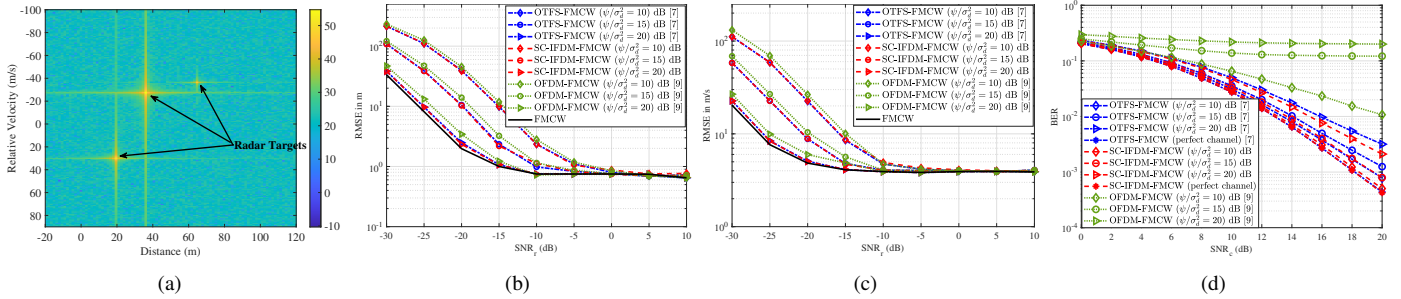


Fig. 4. (a) Range Doppler map (b) Range RMSE performance (multiple targets) (c) Velocity RMSE performance (multiple targets) (d) BER vs SNR.

with the received FMCW signal written as

$$Y^{\text{FMCW}}(k, l) = \sum_{r=0}^{R-1} \sqrt{\psi} \bar{h}_r e^{j2\pi \frac{l(k_r - l_r) + l_r^2 - k_r l_r}{MN}} e^{j2\pi \frac{l^2}{MN}} \quad (17)$$

where  $\bar{h}_r = h_r \Lambda_r(k - k_r, l - l_r)$ . It is observed that the channel shifts the chirp location by  $k_r - l_r$ , causing channel estimation ambiguity, similar to the issue described in orthogonal chirp division multiplexing (OCDM) and discussed in [16].

### C. Proposed Channel Estimation

Due to the behavior of chirps in doubly-selective channels, a novel channel estimation approach is needed. To separate data from the received FMCW pilots, we introduce a transform that extracts every possible chirp in each  $M$  samples as follows

$$\hat{Y}_1(\beta_1, \alpha_1) = \frac{1}{M} \sum_{l=0}^{M-1} Y_{dp}(k, l) e^{-j\pi \frac{(l - \alpha_1 N - \beta_1)}{MN}}, \quad (18)$$

with  $\frac{M}{2} + l + k_r - l_r - k = \alpha_1 N + \beta_1$ , where  $\alpha_1$  and  $\beta_1$  are integers satisfying  $\alpha_1 = 0, \dots, M-1$  and  $\beta_1 = 0, \dots, N-1$ . For each  $\beta_1$ , if  $l_r - k_r = \alpha_1 N + \beta_1$ , the sum becomes

$$\hat{Y}_1(\beta_1, \alpha_1) = \sum_{r=0}^{R-1} \bar{h}_r e^{j\pi \frac{-k_r^2}{MN}} + \hat{Y}^{\text{SC-IFDM}}(\beta_1, \alpha_1) + \hat{W}(\beta_1, \alpha_1), \quad (19)$$

where  $\hat{W}(\beta_1, \alpha_1)$  is the transformed noise. Since the data consist of uniformly distributed QAM symbols with power  $\sigma_d^2$  and zero mean, the expectation  $\mathbf{E} \left[ \sum_{r=0}^{R-1} Y^{\text{SC-IFDM}}(\beta_1, \alpha_1) e^{-j\pi \frac{(l - \alpha_1 N - \beta_1)}{MN}} \right]$  is zero. The variance of  $\hat{Y}_1$  is given as

$$\text{var}\{\hat{Y}_1\} = \frac{\sigma_d^2 (\sum_{r=0}^{R-1} h_r^2) + \sigma^2}{\psi M}. \quad (20)$$

The estimated value  $\hat{Y}_1(\beta_1, \alpha_1)$  is approximately  $\bar{h}_r e^{j\pi \frac{-k_r^2}{MN}}$  for  $l_r \neq k_r$  and  $\sum_{r=0}^{R-1} \bar{h}_r e^{j\pi \frac{-k_r^2}{MN}}$  for  $l_r = k_r$ , which is not sufficient for estimating  $l_r, k_r$  and  $h_r$ . Therefore, in this particular case we consider an extra step to estimate the delay and Doppler shifts where two SC-IFDM symbols are used, one will have an up-chirp and the other a down-chirp. Similarly, a received down-chirp can be given as

$$Y^{\text{FMCW}'}(k, l) = \sum_{r=0}^{R-1} \sqrt{\psi} \bar{h}_r e^{j2\pi \frac{l(k_r + l_r) - l_r^2 - k_r l_r}{MN}} e^{j2\pi \frac{-l^2}{MN}}, \quad (21)$$

which also faces an ambiguity in differentiating delay and Doppler shifts in the case of  $l_r = -k_r$ . However, using the same transform as in (18), we can derive the following

$$\begin{cases} k_r - l_r = \alpha_1 N + \beta_1 \\ k_r + l_r = \alpha_2 N + \beta_2 \end{cases}, \quad (22)$$

where  $\alpha_1, \beta_1$  and  $\alpha_2, \beta_2$  are the estimated shifts from the chirp in symbol 1 and symbol 2, respectively. For each  $\alpha_1, \beta_1$ , we check if a solution for  $\alpha_2, \beta_2$  exists such that the delay and Doppler shifts are integers. Once these shifts are determined, the overlapping channel coefficients can be estimated using a symbol that is not affected by overlap.

## IV. SIMULATIONS RESULTS

In this section, we evaluate the communication and sensing performance of the proposed waveform design. The simulation parameters are configured as follows: a carrier frequency  $f_c$  of 77 GHz, chosen for its high range-Doppler resolution but not restricted to this value, a bandwidth of 200 MHz, and each symbol using  $32 \times 32$  samples. The simulation uses 100 symbols and benchmarks performance against [7], [6], and [9] for both communication and sensing, including a comparison with traditional FMCW for sensing.

For the sensing evaluation, we present the range-velocity plots. The range-velocity map, as shown in Fig. 4(a), is extracted using the conventional radar processing for the proposed JSAC scenario [15]. The simulation targets were placed at distances uniformly distributed between 10 and 80 meters, with velocities ranging between -70 and 70 meters per second.

Fig. 4(b) and 4(c) compare the root mean squared error (RMSE) for range and velocity between the proposed SC-IFDM-FMCW, [6], [9], and traditional FMCW. The proposed JSAC waveform approaches FMCW performance as the power ratio  $\frac{\psi}{\sigma_d^2}$  increases especially at low radar signal-to-noise ratio (SNR) (i.e.  $\text{SNR}_r < 0$  dB), demonstrating robustness across different sensing environments. It performs similarly to OTFS-FMCW due to its sparse and orthogonal chirp representation. SC-IFDM-FMCW outperforms OFDM-FMCW for both range and velocity, as OFDM-FMCW lacks orthogonality between data and chirp, leading to interference.

We assess the bit error rate (BER) versus the communication  $\text{SNR}_c$  performance of the proposed JSAC waveform and compare it with the approaches in [6] and [9]. Fig. 4(d) presents

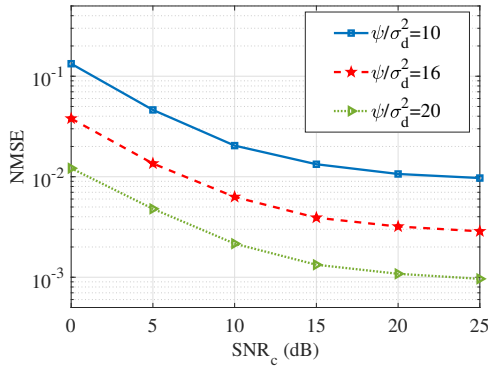


Fig. 5. Channel NMSE performance of the proposed SC-IFDM-FMCW estimation.

BER results for various power ratios ( $\frac{\psi}{\sigma_d^2} \in \{10, 15, 20\}$  dB), considering the proposed channel estimation and perfect channel knowledge for OTFS-FMCW and SC-IFDM-FMCW. The proposed SC-IFDM-FMCW achieves comparable BER to OTFS-FMCW under perfect channel knowledge and surpasses it when using the proposed channel estimation. This improvement mitigates the effects of channel aging, as the radar-based delay and Doppler estimation method in [6] requires numerous symbols to accurately estimate shifts, particularly Doppler, which depends on phase changes. Additionally, SC-IFDM-FMCW outperforms OFDM-FMCW due to its lack of orthogonality and very poor performance in mobile environments. However, as  $\frac{\psi}{\sigma_d^2}$  increases, BER degrades due to higher FMCW interference, emphasizing the critical trade-off between sensing power and communication quality for system optimization.

Fig. 5 illustrates the normalized mean square error (NMSE) performance of the proposed channel estimation technique across varying FMCW and data power levels  $\frac{\psi}{\sigma_d^2}$ . The results show that NMSE improves as the pilot power ratio  $\frac{\psi}{\sigma_d^2}$  increases, reflecting more precise channel estimation. This trend is consistent with the BER performance observed in comparison to the method in [7]. However, the overall BER performance deteriorates due to increased interference power, underscoring the importance of careful optimization to balance sensing and communication efficiency.

## V. CONCLUSION

This paper presents a novel JSAC waveform, SC-IFDM-FMCW, designed to support both communication and sensing. The approach combines SC-IFDM for high data rates and robust mobile performance with FMCW chirp signals for high-resolution sensing, enabling seamless coexistence of both functionalities. The design ensures backward compatibility with existing radar and communication systems, facilitating integration into radar receivers without added complexity. It also addresses challenges like channel aging and interference through an enhanced channel estimation technique, ensuring reliable performance in dynamic environments. Our results show that SC-IFDM-FMCW outperforms OFDM-FMCW in sensing accuracy and surpasses both OFDM-FMCW and OTFS-

FMCW in BER performance. The power ratio  $\frac{\psi}{\sigma_d^2}$  is identified as a critical factor in balancing sensing and communication, highlighting the need for optimization. Future work will optimize waveform parameters, including power ratio, using AI to enhance system performance in real-world conditions. This research positions SC-IFDM-FMCW as a key technology for advancing communication and sensing integration in 6G.

## REFERENCES

- [1] N. C. Luong, X. Lu, D. T. Hoang, D. Niyato, and D. I. Kim, "Radio resource management in joint radar and communication: A comprehensive survey," *IEEE Commun. Surveys Tuts.*, vol. 23, no. 2, pp. 780–814, 2021.
- [2] T. T. Nguyen, K. Elbassioni, N. C. Luong, D. Niyato, and D. I. Kim, "Access management in joint sensing and communication systems: Efficiency versus fairness," *IEEE Trans. Veh. Technol.*, vol. 71, no. 5, pp. 5128–5142, 2022.
- [3] L. Gaudio, M. Kobayashi, G. Caire, and G. Colavolpe, "On the effectiveness of OTFS for joint radar parameter estimation and communication," *IEEE Trans. Wireless Commun.*, vol. 19, no. 9, pp. 5951–5965, 2020.
- [4] S. M. Patole, M. Torlak, D. Wang, and M. Ali, "Automotive radars: A review of signal processing techniques," *IEEE Signal Process. Mag.*, vol. 34, no. 2, pp. 22–35, 2017.
- [5] W. Zhou, R. Zhang, G. Chen, and W. Wu, "Integrated sensing and communication waveform design: A survey," *IEEE Open Journal Commun. Soc.*, vol. 3, pp. 1930–1949, 2022.
- [6] S. E. Zegrar, A. A. Boudjelal, and H. Arslan, "A novel OTFS-Chirp waveform for low-complexity multi-user joint sensing and communication," *IEEE Internet Things J.*, pp. 1–1, 2024.
- [7] S. E. Zegrar, S. Rafique, and H. Arslan, "OTFS-FMCW waveform design for low complexity joint sensing and communication," in *Proc. IEEE 33rd Annu. Int. Symp. Pers., Indoor Mobile Radio Commun. (PIMRC)*, 2022, pp. 988–993.
- [8] J. Xiong, J. Zhu, J. Du, Y. Zhou, C. Yi, and Y. Tang, "An expanded precoding scheme for PAPR reduction in OTFS modulation," in *2024 IEEE Wireless Commun. Netw. Conf. (WCNC)*, 2024, pp. 1–5.
- [9] A. Bouziane, S. E. Zegrar, and H. Arslan, "A novel OFDM-FMCW waveform for low-complexity joint sensing and communication," *IEEE Wireless Commun. Lett.*, pp. 1–1, 2024.
- [10] Y. Fang, L. Tao, and N. Chi, "Interleaved subcarrier allocation for DFT-spread OFDM to reduce PAPR," in *Proc. 17th Opto-Electronics and Communications Conf. (OECC)*, Busan, Korea (South), Jul. 2012, pp. 341–342.
- [11] H. G. Myung, J. Lim, and D. J. Goodman, "Peak-to-average power ratio of single carrier FDMA signals with pulse shaping," in *Proc. IEEE 17th Int. Symp. Pers. Indoor Mobile Radio Commun.*, 2006, pp. 1–5.
- [12] A. Sahin, R. Yang, E. Bala, M. C. Beluri, and R. L. Olesen, "Flexible DFT-S-OFDM: solutions and challenges," *IEEE Commun. Mag.*, vol. 54, no. 11, pp. 106–112, 2016.
- [13] M. W. Chia, B. S. Thian, and T. T. Tjhung, "Distributed DFT-spread OFDM," in *Proc. 10th IEEE Singapore Int. Conf. on Communication Systems (ICCS)*, 2006, pp. 1–5.
- [14] M. Mert Şahin and H. Arslan, "Multi-functional coexistence of radar-sensing and communication waveforms," in *Proc. IEEE Veh. Technol. Conf. (VTC Fall)*, 2020, pp. 1–5.
- [15] S. Kim, I. Paek, and M. Ka, "Simulation and test results of triangular fast ramp FMCW waveform," in *Proc. IEEE Radar Conf. (RADAR)*, 2013, pp. 1–4.
- [16] H. Haif, S. E. Zegrar, and H. Arslan, "Novel OCDM transceiver design for doubly-dispersive channels," *IEEE Trans. Veh. Technol.*, vol. 73, no. 8, pp. 11 237–11 248, 2024.